A stable CoSP/MWCNTs air-diffusion cathode for the photoelectro-Fenton degradation of organic pollutants at pre-pilot scale

Francisco Alcaide[a,*], Garbiñe Álvarez[a], Diego R. V. Guelfi[b], Enric Brillas[b], Ignasi Sirés[b,**]

[a] *CIDETEC, Paseo Miramón 196, 20014 Donostia-San Sebastián, Spain*

[b] *Laboratori d'Electroquímica dels Materials i del Medi Ambient, Departament de Química Física, Facultat de Química, Universitat de Barcelona, Martí i Franquès 1-11, 08028 Barcelona, Spain*

Paper submitted to be published in *Chemical Engineering Journal*

*Corresponding author: Tel.: +34 943309022; fax: +34 94309136.

E-mail address: falcaide@cidetec.es (F. Alcaide)

**Corresponding author: Tel.: +34 934039240; fax: +34 934021231.

E-mail address: i.sires@ub.edu (I. Sirés)

Abstract

CoS_2/MWCNTs have been previously described as potentially viable catalysts to enhance the classical two-electron H_2O_2 production from O_2 reduction reaction (ORR) for in situ water treatment, but their poor stability still limits their large-scale application. Here, the synthesis and characterization of a novel electrocatalyst made of CoSP nanoparticles supported onto multi-walled carbon nanotubes (MWCNTs) is reported. X-ray diffraction data demonstrated the much higher stability conferred upon partial sulfur substitution by phosphorus. Linear and cyclic voltammograms of CoSP/MWCNTs showed a potential window from 0.9 to 0.1 V for the ORR at pH 3.0, along with greater H_2O_2 production ability. Large area air-diffusion cathodes were manufactured by depositing the catalyst onto carbon paper, being further used in a pre-pilot filter-press cell containing a boron-doped diamond anode. A stable H_2O_2 accumulation, with maximum current efficiency of 72.0%, was found upon electrolysis of 2.5 L of 0.050 M Na_2SO_4 at pH 3.0 and 25 mA cm^{-2}. As a crucial finding, Co leaching was negligible. Solutions with 20 mg L^{-1} of the herbicide bentazon in the same electrolyte could not be mineralized by electrochemical oxidation, whereas photoelectro-Fenton with an UVA lamp and 0.50 mM Fe^{2+} led to total removal of the herbicide with 77.0% mineralization.

Keywords: Boron-doped diamond anode; Gas-diffusion electrode; H_2O_2 generation; Pesticide; Photoelectro-Fenton; Water treatment

1. Introduction

H_2O_2 is widely employed in industry, comprising textile, custom synthesis and fine chemicals or pulp and paper sectors [1]. The classical anthraquinone method for H_2O_2 production presents many drawbacks such as the use of toxic organic solvents and stabilizers, which are undesirable for many applications [2]. Furthermore, the handling, storage and transportation of concentrated H_2O_2 solutions is potentially dangerous by their explosion hazard. However, as a green chemical, it is particularly appropriate for the treatment of organic pollutants in synthetic, natural and industrial wastewater by the so-called advanced oxidation processes (AOPs). For these applications, the electrochemical H_2O_2 generation is lately appearing as a less expensive, more environmentally friendly and much safer alternative [2,3]. This approach involves the two-electron O_2 reduction reaction (ORR) at the cathode of the electrolytic cell upon air feeding and current supply [4-6]:

$$O_{2(g)} + 2H^+ + 2e^- \rightarrow H_2O_2 \quad (1)$$

A larger active surface area of the electrode has a direct positive impact on the efficiency of reaction (1). Cathodes made of pristine or chemically modified nanocarbons like carbon nanotubes [7,8], carbon fibers [9] or graphene [10,11] have been recently developed for this purpose. For the electro-Fenton (EF) and photoelectro-Fenton (PEF) processes, the most widespread Fenton-based electrochemical AOPs, the greatest performance in terms of H_2O_2 electrogeneration has been achieved using air-diffusion cathodes [12-16]. In conventional EF, organics are removed by reaction with hydroxyl radical ($^{\bullet}OH$) formed in the bulk from Fenton's reaction (2) between added Fe^{2+} and H_2O_2 produced on site, at optimum pH 3.0. This treatment can be significantly outperformed by PEF upon illumination of the solution with UVA light, since the radiation allows: (i)

a higher •OH production from photo-Fenton reaction (3) that promotes the recycling of Fe^{2+} catalyst from photoreduction of $[Fe(OH)]^{2+}$, the major Fe^{3+} species at pH 3.0; and (ii) the photolysis of photoactive products, including some Fe(III) complexes with final linear carboxylic acids [12,17,18] In an undivided cell, the organics are simultaneously removed by physisorbed hydroxyl radicals formed at the anode surface from water oxidation. At present, boron-doped diamond (BDD) thin-film electrodes are recognized as the best anodes for this reaction route, since they allow the generation of a large quantity of physisorbed BDD(•OH) from reaction (4), being much more active than radicals adsorbed on other anode surfaces [19,20]. In the absence of Fe^{2+} catalyst, the organic matter is destroyed by electrochemical oxidation with electrogenerated H_2O_2 (EO-H_2O_2), which is usually less powerful than EF and PEF.

$$Fe^{2+} + H_2O_2 \rightarrow Fe^{3+} + {}^{\bullet}OH + OH^- \quad (2)$$

$$[Fe(OH)]^{2+} + h\nu \rightarrow Fe^{2+} + {}^{\bullet}OH \quad (3)$$

$$BDD + H_2O \rightarrow BDD({}^{\bullet}OH) + H^+ + e^- \quad (4)$$

Commercial air-diffusion cathodes are usually made of raw carbonaceous materials, most typically hydrophobic carbon black particles. Nonetheless, the removal of organic contaminants of emerging concern (OCECs) currently detected in complex water matrices requires the use of more advanced cathodes with superior characteristics like biofouling resistance, stability and endurance, but still maintaining or even improving the ability for H_2O_2 production. Lately, the possibility to use carbonaceous materials as support to disperse other catalytic materials has been explored, especially with nonprecious metal-based electrocatalysts [3]. Among them, Co-based nanoparticles have been sorted out as suitable candidates because of their excellent electrocatalytic properties [21,22]. CoS_2-based particles have been employed for the efficient H_2 evolution from

water [23] and ORR with high selectivity toward H_2O_2 [24,25], although several authors have recently described a better performance for both reactions upon doping with phosphorus (i.e., CoSP-based electrocatalysts) [26-30]. This has been mainly attributed to the fact that P atoms may improve the chemical stability of the pyrite-type CoS_2 structure. Phosphorous incorporation mitigates sulfate formation, rendering CoS_2 particles more stable against oxidation [26]. Apparently, the substitution of S by P does not cause any significant alteration of the crystal structure or lattice parameters, thanks to the very similar atomic sizes of both atoms.

We have previously examined the properties of 3-cm^2 air-diffusion cathodes made of nanocrystalline CoS_2 deposited onto carbon paper to degrade acidic solutions of the anaesthetic tetracaine by PEF [31]. However, cathodes with better electroactivity for H_2O_2 electrogeneration and greater stability, as well as testing at a larger scale, are required to correctly evaluate the viability of this kind of materials for the destruction of organic pollutants from water.

This article reports the preparation of novel air-diffusion cathodes made of CoSP/multi-walled carbon nanotubes (MWCNTs) on carbon paper, with large surface area, along with the structural, chemical and electrochemical characterization of the electrocatalysts. To clearly describe the advantages of the new material, CoS_2/MWCNTs were prepared and characterized as well. The ability of the P-doped cathodes to produce H_2O_2 was studied in a 2.5 L pre-pilot plant with 0.050 M Na_2SO_4 as supporting electrolyte at pH 3.0. Then, their application to EO-H_2O_2 and PEF processes was tested in the pre-pilot setup by treating an acidic solution of bentazon ($C_{10}H_{12}N_2O_3S$, 3-isopropyl-1H-2,1,3-benzothiadiazin-4(3H)-one-2,2-dioxide, M = 240.3 g mol^{-1}), a very recalcitrant herbicide detected at concentrations up to 120 μg L^{-1} in groundwater [32] and 28 μg L^{-1} in surface water [33].

2. Materials and methods

2.1. Chemicals

Reagent grade sodium sulfate, sodium hypophosphite monohydrate, sulfur, sodium thiosulfate pentahydrate, iron(II) sulfate heptahydrate (> 98%), cobalt(II) chloride hexahydrate, sulfuric acid and nitric acid were purchased from VWR, Scharlau and Sigma-Aldrich. MWCNTs were purchased from Cheap Tubes Inc. (outer diameter < 8 nm, length 10-30 μm, 3.86 wt.% of COOH content). Extra pure 2-propanol and 5 wt.% Nafion® perfluorinated resin solution were purchased from Scharlau and Sigma-Aldrich, respectively. Bentazon (> 99%) was purchased from Sigma-Aldrich. Synthetic and analytical solutions were prepared with Millipore Milli-Q water (resistivity > 18.2 MΩ cm), whereas the electrolyte and herbicide solutions treated in the pre-pilot plant were prepared with deionized water.

2.2. Synthesis of CoSP/MWCNTs catalyst and electrode manufacturing

The first step involved the preparation of the CoS_2/MWCNTs catalyst using 2:2:1 molar proportion of Co(II) chloride hexahydrate, sodium thiosulfate pentahydrate and sulfur, which were mixed so as to obtain 50 wt.% CoS_2 supported in MWCNTs, employing a 250 mL PTFE autoclave with its 80% volume filled with Milli-Q water [34]. The device was kept at 140 ºC for 24 h, and then it was cooled down to room temperature. The resulting powder was filtered, washed several times with carbon sulfide, ethanol and water, and finally dried in an oven at 80 ºC.

In a second step, about 500 mg of a fresh CoS_2/MWCNTs catalyst were impregnated with 280 mg of sodium hypophosphite monohydrate as phosphorus precursor in order to obtain a 1:1:1 atomic ratio between Co, S and P. Phosphorus doping of the CoS_2 was achieved upon thermal treatment at 400 ºC for 1 h under argon stream.

O_2- and air-diffusion cathodes of 30 cm^2 geometric area (6 cm × 5 cm) were prepared by the spraying method [35]. The selected catalysts were dispersed in an appropriate mixture of Milli-Q water, ethanol and Nafion® solution by ultrasonication. The resulting ink was sprayed several times onto a carbon paper diffusion layer (Freudenberg H23C4, 255 μm thickness) using an air-brush gun fed with pure nitrogen and the resulting material was dried in an oven at 60 ºC to finally obtain a gas-diffusion electrode. Electrodes with a catalyst loading of 2.0 mg cm^{-2} and a Nafion® content of 30 wt.% in dry weight were obtained.

2.3. Physicochemical characterization of catalysts

The X-ray diffraction (XRD) analysis was made using a Bruker D8 Advance diffractometer, with Cu K_α radiation and a 2θ scan from 15° to 60° (at 1° min^{-1}). The average crystallite sizes were determined by the Scherrer equation, using the (200), (210) and (211) Bragg reflection peaks. Scanning electron microscopy (SEM) analysis was performed with a JEOL JSM5910-LV microscope. Field emission SEM (FE-SEM) analysis including elemental mapping was carried out using a Zeiss Ultra Plus microscope. Co:S and Co:S:P atomic ratios, along with the mass ratio of the elements to carbon in the catalysts, were determined by energy dispersive X-ray (EDX) technique, using an INCA Energy 300 detector coupled to the SEM microscope. The reported compositions are the average of five different measurements on the same sample, with relative error < 1 %.

2.4. Electrochemical characterization of electrocatalysts

Cyclic and linear sweep voltammetries were recorded using a PARSTAT 2273 potentiostat from Ametek, Inc., driven by the PowerSuite software (version 2.58), in a conventional three-electrode glass cell thermostatized at 25.0 ºC. Potentials were measured against a reversible hydrogen electrode (RHE) from Gaskatel GmbH in contact

with the electrolyte through a Luggin capillary. The counter electrode was a platinum wire. The working electrode was a 0.07069 cm^2 glassy carbon tip connected to a rotating disk electrode (RDE), model EDI101, from Radiometer Analytical. The working electrode was modified as follows: 1 mg of catalyst was dispersed in 500 μL of a 1:1 (v/v) 2-propanol/Milli-Q water mixture, then sonicated for 30 min and the resulting ink was transferred onto the surface of the glassy carbon disk. Once dried under nitrogen stream, 5 μL of Nafion® solution was dropped onto the catalyst layer to fix it, achieving a catalyst loading of 80 μg cm^{-2}. Prior to each use, the glassy carbon disk was polished to a mirror finish using alumina powder suspensions (0.3 μm and 0.05 μm from Buehle), followed by sonication in water. Cyclic voltammograms were recorded with 50 mL of 0.050 M Na_2SO_4 at pH 3.0 at a scan rate of 20 mV s^{-1}. The electrolyte was deaerated by bubbling nitrogen for 20 min prior to the experiments, which was further maintained over the solution. Linear sweep voltammograms were measured after O_2-saturation of the solution with pure gas by bubbling it for 30 min. The *j-E* curves were recorded at rotation rates between 400 and 2500 rpm, and scan rate of 5 mV s^{-1}, to keep steady conditions at the surface of the working electrode. The *j* values are given considering the geometrical area of the working electrode and all the *j-E* curves have been corrected by the *IR*-drop in the electrolyte solution, using the *eis* technique.

2.5. Assays in the pre-pilot flow plant

The manufactured air-diffusion cathodes modified with the CoS_2/MWCNTs or the CoSP/MWCNTs catalyst were employed for the H_2O_2 generation and the treatment of bentazon solutions by EAOPs. These assays were carried out in a 2.5 L pre-pilot plant constructed in our laboratory. A scheme of this plant is shown in earlier work [36]. Briefly, the electrolyzed solution was recirculated under the action of a peristaltic pump. From the reservoir, it passed through a rotameter used to keep the liquid flow rate at 180

L min^{-1}, two heat exchangers to maintain the temperature at 35 ºC, the electrochemical reactor and the annular glass photoreactor, before being returned to the reservoir. The filter-press electrochemical cell was equipped with two parallel electrodes of 20 cm^2 area in contact with the solution, with 1.2 cm of interelectrode gap. The anode was a BDD thin film deposited on a Si wafer, purchased from NeoCoat. The air-diffusion cathode prepared with carbon paper as described above was fed with air at 8.6 kPa of overpressure. An N5746A System DC power supply from Agilent Technologies was utilized to provide a constant current to the electrodes. This apparatus also displayed the cell voltage (E_{cell}). In PEF process, a 27E 160-W UVA lamp of λ_{max} = 360 nm from Omnilux, placed at the center of the annular photoreactor with 640 mL irradiated volume, always remained switched on. In contrast, this lamp was switched off during the EO-H_2O_2 treatment and the plant was covered with an opaque plastic to impede natural light irradiation.

All the electrolytic assays were performed with 0.050 M Na_2SO_4 at pH 3.0 as the electrolyte, being this pH value the optimum one for Fenton's reaction (2) in PEF treatment [4]. A catalyst concentration of 0.50 mM Fe^{2+} was selected since it is the most typical using air-diffusion cathodes [36,37]. Before using a fresh cathode, the activation of its surface was achieved by electrolyzing 2.5 L of 0.050 M Na_2SO_4 at pH 3.0 and 35 ºC, employing a BDD anode at 50 mA cm^{-2} for 360 min. Reproducible H_2O_2 values were obtained after three consecutive runs under such conditions, and a good stability of the activated CoSP/MWCNTs cathode was found in further application, as assessed from Co leaching to solution. Therefore, it was unnecessary to pretreat or reactivate the cathode before each subsequent use.

2.6. Analytical procedures

The solution pH was adjusted to 3.0 with H_2SO_4 and monitored on a Crison GLP 22 pH-meter. The H_2O_2 concentration was determined by the metavanadate method using a

Shimadzu 1800 UV/Vis spectrophotometer at λ = 450 nm [38]. Samples withdrawn from solutions were filtered with Whatman 0.45 μm PTFE filters before analysis. The dissolved total organic carbon (TOC) was immediately determined upon injection of 50 μL aliquots into a Shimadzu VCSN TOC, with ±1% reproducibility. The bentazon concentration was measured by reversed-phase HPLC. Before this, the sample (0.5 mL) was immediately diluted 1:1 (v/v) with acetonitrile to stop the degradation process. Then, 10 μL aliquots were filtered with a 0.45 μm PTFE filter and injected into a Waters 600 LC coupled to a Waters 996 photodiode array detector. The LC contained a BDS Hypersil C18 6 μm (250 mm × 4.6 mm) column and a 3:7 (v/v) 10 mM KH_2PO_4 (pH 3)/acetonitrile mixture was eluted at 0.8 mL min^{-1} as mobile phase. Bentazon displayed a well-defined peak at retention time of 4.7 min and its concentration was measured at λ = 242 nm. Duplicate trials were made to assess the mineralization and concentration decays of bentazon, and average values are given. NH_4^+, NO_3^- and SO_4^{2-} contents generated along the treatments were determined as reported elsewhere [39]. The cobalt released to the solution was measured by inductively coupled plasma-optical emission spectrometry (ICP-OES) on a Perkin Elmer Optima 3200 L spectrometer.

3. Results and discussion

3.1. Structural and chemical analysis of catalysts

The synthesized CoS_2/MWCNTs and CoSP/MWCNTs catalysts were analyzed by XRD, FE-SEM and EDX techniques. Fig. 1a and b present the X-ray diffraction patterns for both supported catalysts. As can be seen, both spectra showed peaks that can be associated with the (111), (200), (210), (211), (220), (311), (023) and (321) planes of the pyrite-type crystal structure, according to the JCPDS card No. 41-1471. This constitutes a crucial structural finding, since it means that phosphorus atoms are incorporated in

substitutional positions in the CoSP crystal lattice, thus replacing half of the S atoms present in the case of CoS_2 crystals. The average crystallite sizes were 27.9 ± 2.0 nm and 25.6 ± 3.2 nm for CoS_2/MWCNTs and CoSP/MWCNTs catalysts, respectively.

The stability of both catalysts was also evaluated by XRD. The results demonstrated that the presence of phosphorus atoms induced a much greater crystal stability. Fig. 1a shows the diffractograms corresponding to the as-synthesized CoS_2/MWCNTs, which underwent an evident degradation within some few weeks when the particles were stored under atmospheric conditions. Peaks corresponding to CoS_2 tended to disappear, whereas some new peaks appeared due to the decomposition of cobalt disulfide and formation of sulfate groups. It is noticeable that, within the first 4 weeks, some little peaks appeared around 2θ values of 18º and 26º, in agreement with the presence of sulfate groups, although they remained stable during further catalyst analysis in subsequent weeks, since the increase in their intensity was insignificant. In contrast, when the catalyst was stored under an inert atmosphere provided by nitrogen gas, its stability was greatly enhanced, as depicted in Fig. 2, which suggests that exposure to O_2 in contact with atmospheric air is highly detrimental due to gradual oxidation. On the other hand, when phosphorus was incorporated during the synthesis, the stability of the manufactured catalyst increased dramatically, impeding its decomposition for at least 12 weeks (see Fig. 1b). Due to the high stability of the CoSP/MWCNTs catalyst, it was unnecessary to store it under nitrogen atmosphere, which is clearly advantageous for handling.

The morphology of the catalysts was characterized by FE-SEM. Fig. 3a and b reveal that CoS_2/MWCNTs and CoSP/MWCNTs contained nanocrystals with a cubic-like morphology, respectively, in which the CoS_2 and CoSP dispersion was strongly enhanced by the presence of the multi-walled carbon nanotubes as underlying platform, which

prevented the aggregation of particles. This is a key finding to ensure the homogeneity of cathodes to be prepared.

The chemical analysis of both catalysts was performed by EDX. From the spectrum of Fig. 4a, an 1:2 Co:S atomic ratio for CoS_2/MWCNTs was confirmed, which agreed with the CoS_2 pyrite-phase identified from XRD analysis. Moreover, a 46 wt.% of CoS_2 content in the CoS_2/MWCNTs catalyst was determined, very close to the nominal value of 50 wt.%. In the case of the CoSP/MWCNTs catalyst, the EDX mapping of Fig. 5 highlights uniform deposition of the elements Co, S and P onto the nanocarbonaceous support, which corroborates the incorporation of P in substitutional positions rather than as a segregated phase. From this finding and the corresponding EDX spectrum of Fig. 4b, an atomic content of 26% for Co, 33% for S and 30% for P was obtained, being quite close to the expected 1:1:1. The rest was related to C from the nanotubes support.

3.2. Electrochemical characterization of catalysts

Cyclic voltammetric measurements were carried out for the CoSP/MWCNTs catalyst in N_2-saturated and O_2-saturated 0.050 M Na_2SO_4 solution at pH 3.0. Fig. 6 depicts the cyclic voltammograms recorded in inert atmosphere, curves *a* and *b*, corresponding to 5th and 10th cycle, respectively. It has been previously reported that for CoS_2 black catalyst in 0.1 M $HClO_4$, the cathodic reduction of the oxidized CoS_2 surface and the oxidation of cobalt disulfide to cobalt sulfate species (at $E > 0.600$ V vs. RHE) affects negatively its stability during the first scans of cyclic voltammetry experiments [24]. Such behavior is not shown for the CoSP catalyst in Fig. 6, since no apparent differences appear between curves *a* and *b*. This means that the presence of phosphorus stabilizes the Co-based nanoparticles, with an evident decrease of the abovementioned faradaic processes. This is a very noteworthy consequence of the incorporation of P in the crystal lattice, paving the way for the preparation of stable air-diffusion cathodes. Additionally, one can observe

in the curve *c* of Fig. 6 that the onset potential for the ORR in the O_2-saturated electrolyte was located around 0.9 V vs. RHE, with a wide potential window reaching about 0.1 V vs. RHE.

Based on the above results, the ORR on CoSP/MWCNTs electrocatalyst was studied in an O_2-saturated 0.050 M Na_2SO_4 solution at pH 3.0 by linear sweep voltammetry within a potential range from 0.840 to 0.200 V vs. RHE using an RDE setup. For comparison, the voltammetric response of CoS_2/MWCNTs electrocatalyst was also investigated. The voltammograms were recorded at rotation rates between 400 and 2500 rpm, as depicted in Fig. 7a and b, respectively. In both cases, the desired electrocatalytic activity towards the ORR can be observed. Note that greater current densities and less positive potentials were obtained as the rotation rate was increased, especially for the CoSP/MWCNTs catalyst. Moreover, the half-wave potential ($E_{1/2}$) shifted qualitatively towards more negative values, which is indicative of a totally irreversible redox reaction.

Previous work [24] pointed out that the ORR on CoS_2, either as black catalyst or supported on carbon nanotubes, yielded H_2O_2 with $n = 2$, particularly at reduction potentials $E \leq 0.250$ V vs. RHE. To confirm this point for our prepared catalysts, Koutecky-Levich analysis was carried out, thus gaining further insight into the kinetics of the ORR on their surface. Fig. 8 depicts the inverse of the current density (j^{-1}) at a reduction potential of 0.250 V against the inverse of the square root of the rotation rate ($\omega^{-1/2}$), using the data extracted from the experimental curves of Fig. 7. Excellent linear fittings between both parameters can be seen in both cases and, even more relevant, the non-zero intercepts points towards kinetic limitations of the ORR on both catalysts. Worth mentioning, higher *j* values were obtained with the CoSP/MWCNTs catalyst at any given rotation rate. The number of electrons (*n*) transferred per O_2 molecule was then estimated from the slope of the Koutecky-Levich plots of Fig. 8 via Eq. (5) [40]:

$$\frac{1}{j}=\frac{1}{j_k}+\frac{1}{j_l}=\frac{1}{nFkC_{O_2}^b}+\frac{1}{0.62nFC_{O_2}^b D_{O_2}^{2/3}\upsilon^{-1/6}\omega^{1/2}} \quad (5)$$

where j_k represents the kinetic current density and j_l, denotes the diffusion limiting current density. Apart from the Faraday constant *F*, the other terms are: the reaction rate constant *k*, the O_2 solubility $C_{O_2}^b$ (1.1 mM), the O_2 diffusion coefficient D_{O_2} (1.7×10^{-5} cm^2 s^{-1}) and the kinematic viscosity of the solution υ (0.01 cm^2 s^{-1}).

A transferred number of electrons (*n*) of 1.5 and 1.9 was obtained for the CoS_2/MWCNTs and CoSP/MWCNTs electrocatalysts at 0.250 V, respectively. Considering the approaches made for the $C_{O_2}^b$, D_{O_2} and υ, values taken for pure water, one can conclude that the true *n*-value is 2 for both materials, thus confirming the ability of these kinds of Co-based catalysts to form H_2O_2 as the final product at adequate potential values. This agrees with the behavior of some cobalt sulfides for which the two-electron ORR is the dominant reaction pathway, especially at specific cathodic *E* values [41]. Note that, for comparison, Fig. 8 also depicts the theoretical j^{-1} vs. $\omega^{-1/2}$ linear plots that should be expected assuming $n = 2$ (O_2 reduction to H_2O_2) or $n = 4$ (O_2 reduction to H_2O), clearly evidencing that the slopes of the Koutecky-Levich plots matched with that of the plot at $n = 2$.

3.3. H_2O_2 electrogeneration in the pre-pilot plant

Although the electrochemical characterization of the catalysts showed an excellent ability for H_2O_2 generation at small scale, it is crucial from a technical point of view to clarify if they can be used at large scale as stable air-diffusion cathodes. This was corroborated by testing the behavior of 20-cm^2 cathodes made of CoS_2/MWCNTs or CoSP/MWCNTs catalysts deposited onto carbon paper. Each cathode was placed in a filter-press cell that also contained a 20-cm^2 BDD anode and its performance was assessed using a pre-pilot plant under circulation of 2.5 L of 0.050 M Na_2SO_4 solutions at pH 3.0

and 35 ºC. First, the electrodes were activated at 50 mA cm^{-2} for 360 min and, after three cycles, reproducible H_2O_2 concentrations were already obtained. Co analysis of the electrolyzed solutions evidenced the leaching of about 9% of the initial value of each cathode during the activation process, but no metal (or below LOD = 0.02 mg L^{-1}) was detected in any of the subsequent electrolyses, showing that both air-diffusion electrodes had become stabilized.

Fig. 9a illustrates the time course of the accumulated H_2O_2 content during the trials performed at 25 mA cm^{-2} using the cathodes once stabilized. A rapid and continuous rise of H_2O_2 concentration can be always observed, attaining 11.8 mM using CoS_2/MWCNTs and a greater value of 12.8 mM with CoSP/MWCNTs, after 360 min. An uncatalyzed MWCNTs air-diffusion cathode yielded a much lower H_2O_2 content of 7.7 mM. This corresponds to a 1.53-fold and 1.66-fold increase of H_2O_2 concentration when the MWCNTs were modified with CoS_2 or CoSP, respectively. The superiority of the latter cathode was confirmed from the resulting higher current efficiency (CE), determined from the Faraday law. Fig. 9b reveals that CE dropped from 72.0% to 52.6% using CoSP/MWCNTs and from a lower value of 54.0% to 45.7% using CoS_2/MWCNTs. The drop was more evident, from 47.9% to 34.3%, using the uncatalyzed MWCNTs. The decay of CE as the electrolysis time was prolonged can be related to the progressively larger occurrence of H_2O_2 decomposition as its concentration increased. This compound is expected to be oxidized to O_2 at the BDD anode, since an undivided reactor was employed and this caused its partial disappearance from the solution [4,6]. Considering that during the early stages of H_2O_2 accumulation trials the abovementioned decomposition reactions were rather insignificant, the CE values directly inform about the selectivity of the material towards H_2O_2 electrogeneration. Hence, the CoSP/MWCNTs cathode presented the higher selectivity (72.0%), which decreased for

CoS_2/MWCNTs and MWCNTs cathodes. The selectivity lower than 100% is due to the existence of concomitant cathodic reductions, such as H^+ to H_2 gas and/or the 4-electron reduction of O_2 gas [4-6].

The aforementioned findings demonstrate that the CoSP/MWCNTs was the best electrocatalyst for H_2O_2 generation in the absence of organic pollutants. To show that the air-diffusion cathode modified with P atoms can be used in EAOPs, a comparative assay was made by measuring the H_2O_2 accumulation when the above electrolyte contained 20 mg L^{-1} of bentazon and 0.50 mM Fe^{2+}, being treated under PEF conditions. The H_2O_2 consumption from Fenton's reaction (2) led to its drastic decay in solution, only reaching 2.0 mg L^{-1} at 360 min (see Fig. 9a), with a fluctuating CE value between 14.3% and 9.0% (see Fig. 9b). These results demonstrate that the CoSP/MWCNTs-modified cathode is able to produce H_2O_2 concentration at sufficient concentration to yield the maximum amount of $^{\bullet}OH$ in Fenton-based processes.

3.4. Electrochemical treatment of bentazon solutions in the pre-pilot plant

The degradation and mineralization of 2.5 L of 20 mg L^{-1} bentazon solutions in 0.050 M Na_2SO_4 at pH 3.0 was assessed using the filter-press cell with a BDD anode and the stabilized CoSP/MWCNTs air-diffusion cathode. The performance of EO-H_2O_2 and PEF with 0.50 mM Fe^{2+} was compared at a low *j* value of 25 mA cm^{-2}. Under these conditions, Fig. 10a shows a very slow herbicide abatement using EO-H_2O_2 since only 53.6% reduction was achieved at 360 min. This suggests that bentazon molecules are quite refractory to the attack of the main oxidant BDD($^{\bullet}OH$), formed from reaction (4), as well as weaker oxidants like H_2O_2. In contrast, Fig. 10a also highlights that PEF led to total disappearance of the herbicide in only 20 min, as expected if $^{\bullet}OH$ generated from reactions (2) and (3) attacks very rapidly all bentazon molecules. The inset of Fig. 10a depicts the good linear plots obtained assuming a pseudo-first-order kinetics in both

cases, allowing the determination of an apparent rate constant of 0.0030 min^{-1} (R^2 = 0.989) in EO-H_2O_2, much smaller than 0.1875 min^{-1} (R^2 = 0.980) obtained in PEF. This behavior suggests a constant and small production of the main reactive oxidizing agents (BDD(•OH) and/or •OH) during each treatment.

The mineralization degree attained in the above treatments was determined from the decay of solution TOC. The TOC reduction was lower than 3% in EO-H_2O_2 (data not shown), in agreement with the small herbicide removal by BDD(•OH) depicted in Fig. 10a. In PEF, Fig. 10b shows a fast mineralization up to 62.2% at 90 min, followed by a much slower TOC abatement to attain 77.0% at 240 min. At longer time, no additional mineralization occurred, probably due to the formation of final products that are highly stable to the attack of BDD(•OH), •OH and UVA light. The electric energy consumption required in the PEF system (with average E_{cell} = 12.5 V) until 240 min of electrolysis was 10.1 kWh m^{-3}. The energy required by the 160-W UVA lamp is not consider here, since actually the alternative application of solar PEF (SPEF), with free sunlight irradiation, could be chosen as more cost-effective process in practice [13,15,18].

The inorganic ions produced during the mineralization of the 20 mg L^{-1} bentazon solutions were identified and quantified at the end of the PEF treatment. The initial S (0.082 mM) was transformed into 99% of SO_4^{2-} ion, whereas the initial N (0.164 mM) was converted into 11.5% and 70.5% of NH_4^+ and NO_3^- ions, respectively. Considering that mineralization involves the formation of CO_2, along with NO_3^- and SO_4^{2-} as main ions, the following total reaction for the pesticide can be envisaged:

$$C_{10}H_{12}N_2O_3S + 27H_2O \rightarrow 10CO_2 + 2NO_3^- + SO_4^{2-} + 66H^+ + 62e^- \quad (6)$$

The percentage of mineralization current efficiency (MCE) was then estimated from the TOC abatement (△TOC, mg L^{-1}) via Eq. (7) [4]:

$$\mathrm{MCE} = \frac{n\,F\,V\Delta\mathrm{TOC}}{4.32\mathrm{x}10^{7} m\,I\,t}100 \quad (7)$$

where n = 62 is the number of electrons consumed in reaction (6), V is the solution volume (L), 4.32×10^{7} is a conversion factor to homogenize the units, m = 10 is the number of carbon atoms of bentazon, I is the applied current (A) and t is the time (h).

The inset of Fig. 10b highlights a dramatic drop of MCE from 38.8% during the first stages of PEF to 13.2% at 240 min, because of the large formation of recalcitrant products and the loss of organic load [4,6].

No Co was detected in the above treated solutions, confirming the large stability of the CoSP/MWCNTs cathode used. Furthermore, the profile for H_2O_2 accumulation in 0.050 M Na_2SO_4 at pH 3.0 and j = 25 mA cm^{-2} determined with the CoSP/MWCNTs cathode after use in the degradation trials was practically the same as that shown in Fig. 9a. This corroborates not only the enhanced stability of the air-diffusion cathodes, but also their great ability to be used in consecutive PEF treatments with invariable efficiency.

4. Conclusions

In summary, novel air-diffusion cathodes composed of CoSP/MWCNTs electrocatalysts deposited onto carbon paper are more stable than those containing CoS_2/MWCNTs at ambient conditions. Voltammetric studies demonstrated that the ORR occurred at the CoSP/MWCNTs surface in the range from 0.9 to 0.1 V, with a large ability to generate H_2O_2 via a two-electron reduction of O_2. This was confirmed in a pre-pilot plant with a BDD anode and a CoSP/MWCNTs air-diffusion cathode, both of large area, at 25 mA cm^{-2}, allowing maximum current efficiencies of 72.0%. In these trials, the cathode showed a large stability without significant Co leaching. The good mineralization

with acceptable MCE values obtained in this work for bentazon removal suggests that the novel and highly stable CoSP/MWCNTs cathode can be potentially viable for the PEF treatment of organic pollutants in acidic wastewater at real scale.

Acknowledgments

The authors gratefully acknowledge financial support from projects CTQ2013-48897-C2-1-R, CTQ2013-48897-C2-2-R and CTQ2016-78616-R (AEI/FEDER, EU).

References

[1] J.M. Campos-Martín, G. Blanco-Brieva, J.L. Fierro, Hydrogen peroxide synthesis: an outlook beyond the anthraquinone process, Angew. Chem. Int. Ed. 45 (2006) 6962-6984.

[2] S. Yang, A. Verdaguer-Casadevall, L. Arnarson, L. Silvioli, V. Čolić, R. Frydendal, J. Rossmeisl, I. Chorkendorff, I.E.L. Stephens, Toward the decentralized electrochemical production of H_2O_2: a focus on the catalysis, ACS Catal. 8 (2018) 4064-4081.

[3] M. Shao, Q. Chang, J.-P. Dodelet, R. Chenitz, Recent advances in electrocatalysts for oxygen reduction reaction, Chem. Rev. 116 (2016) 3594-3657.

[4] E. Brillas, I. Sirés, M.A. Oturan, Electro-Fenton process and related electrochemical technologies based on Fenton's reaction chemistry, Chem. Rev. 109 (2009) 6570-6631.

[5] M.A. Oturan, J.-J. Aaron, Advanced oxidation processes in water/wastewater treatment: principles and applications. A review, Crit. Rev. Environ. Sci. Technol. 44 (2014) 2577-2641.

[6] C.A. Martínez-Huitle, M.A. Rodrigo, I. Sirés, O. Scialdone, Single and coupled electrochemical processes and reactors for the abatement of organic water pollutants: a critical review, Chem. Rev. 115 (2015) 13362-13407.

[7] H. Roth, Y. Gendel, P. Buzatu, O. David, M. Wessling, Tubular carbon nanotube-based gas diffusion electrode removes persistent organic pollutants by a cyclic adsorption – Electro-Fenton process, J. Hazard. Mater. 307 (2016) 1-6.

[8] F. Yu, Y. Chen, H. Ma, Ultrahigh yield of hydrogen peroxide and effective diclofenac degradation on a graphite felt cathode loaded with CNTs and carbon black: an electro-generation mechanism and a degradation pathway, New J. Chem. 42 (2018) 4485-4494.

[9] K.V. Plakas, A.J. Karabelas, S.S. Sklari, V.T. Zaspalis, Toward the development of a novel electro-Fenton system for eliminating toxic organic substances from water. Part 1. In situ generation of hydrogen peroxide, Ind. Eng. Chem. Res. 52 (2013) 13948-13956.

[10] T.X.H. Le, M. Bechelany, M.S. Lacour, N. Oturan, M.A. Oturan, M. Cretin, High removal efficiency of dye pollutants by electron-Fenton process using a graphene based cathode, Carbon 94 (2015) 1003-1011.

[11] W. Yang, M. Zhou, J. Cai, L. Liang, G. Ren, L. Jiang, Ultrahigh yield of hydrogen peroxide on graphite felt cathode modified with electrochemically exfoliated graphene, J. Mater. Chem. A 5 (2017) 8070-8080.

[12] A. Thiam, I. Sirés, J.A. Garrido, R.M. Rodríguez, E. Brillas, Decolorization and mineralization of Allura Red AC aqueous solutions by electrochemical advanced oxidation processes, J. Hazard. Mater. 290 (2015) 34-42.

[13] X. Yu, M. Zhou, G. Ren, L. Ma, A novel dual gas diffusion electrodes system for efficient hydrogen peroxide generation used in electro-Fenton, Chem. Eng. J. 263 (2015) 92-100.

[14] A. Galia, S. Lanzalaco, M.A. Sabatino, C. Dispenza, O. Scialdone, I. Sirés, Crosslinking of poly(vinylpyrrolidone) activated by electrogenerated hydroxyl radicals: a first step towards a simple and cheap synthetic route of nanogel vectors, Electrochem. Commun. 62 (2016) 64-68.

[15] S. Lanzalaco, I. Sirés, M.A. Sabatino, C. Dispenza, O. Scialdone, A. Galia, Synthesis of polymer nanogels by electro-Fenton process: investigation of the effect of main operation parameters, Electrochim. Acta. 246 (2017) 812-822.

[16] T. Pérez, G. Coria, I. Sirés, J.L. Nava, A.R. Uribe, Electrosynthesis of hydrogen peroxide in a filter-press flow cell using graphite felt as air-diffusion cathode, J. Electroanal. Chem. 812 (2018) 54-58.

[17] A. Thiam, E. Brillas, J.A. Garrido, R.M. Rodríguez, I. Sirés, Routes for the electrochemical degradation of the artificial food azo-colour Ponceau 4R by advanced oxidation processes, Appl. Catal. B: Environ. 180 (2016) 227-236.

[18] G. Coria, T. Pérez, I. Sirés, E. Brillas, J.L. Nava, Abatement of the antibiotic levofloxacin in a solar photoelectro-Fenton flow plant: modeling the dissolved organic carbon concentration-time relationship, Chemosphere 198 (2018) 174-181.

[19] G. Coria, I. Sirés, E. Brillas, J.L. Nava, Influence of the anode material on the degradation of naproxen by Fenton-based electrochemical processes, Chem. Eng. J. 304 (2016) 817-825.

[20] J.R. Steter, E. Brillas, I. Sirés, On the selection of the anode material for the electrochemical removal of methylparaben from different aqueous media, Electrochim. Acta 222 (2016) 1464-1474.

[21] M.S. Faber, R. Dziedzic, M.A. Lukowski, N.S. Kaiser, Q. Ding, S. Jin, High-performance electrocatalysis using metallic cobalt pyrite (CoS_2) micro- and nanostructures, J. Am. Chem. Soc. 136 (2014) 10053-1006.

[22] S. Anantharaj, S.R. Ede, K. Sakthikumar, K. Karthick, S. Mishra, S. Kundu, Recent trends and perspectives in electrochemical water splitting with an emphasis on sulfide, selenide, and phosphide catalysts of Fe, Co, and Ni: a review, ACS Catal. 6 (2016) 8069-8097.

[23] C.-J. Chen, P.-T. Chen, M. Basu, K.-C. Yang, Y.-R. Lu, C.-L. Dong, C.-G. Ma, C.-C. Shen, S.-F. Hu, R.-S. Liu, Integrated cobalt disulfide (CoS_2) Co-catalyst passivation layer on silicon microwires for photoelectrochemical hydrogen evolution, J. Mater. Chem. A 3 (2015) 23466-23476.

[24] J.S. Jirkovský, A. Björling, E. Ahlberg, Reduction of oxygen on dispersed nanocrystalline CoS_2, J. Phys. Chem. C 116 (2012) 24436-24444.

[25] D.C. Higgins, F.M. Hassan, M.H. Seo, J.Y. Choi, M.A. Hoque, D.U. Lee, Z. Chen, Shape-controlled octahedral cobalt disulfide nanoparticles supported on nitrogen and sulfur doped graphene/carbon nanotube composites for oxygen reduction in acidic electrolyte, J. Mater. Chem. A 3 (2015) 6340-6350.

[26] W. Liu, E. Hu, H. Jiang, Y. Xiang, Z. Weng, M. Li, Q. Fan, X. Yu, E.I. Altman, H. Wang, A highly active and stable hydrogen evolution catalyst based on pyrite-structured cobalt phosphosulfide, Nature Commun. 7 (2016) 10771.

[27] Y. Zhou, R. Ma, S.L. Candelaria, J. Wang, Q. Liu, E. Uchaker, P. Li, Y. Chen, G. Cao, Phosphorus/sulfur Co-doped porous carbon with enhanced specific capacitance for supercapacitor and improved catalytic activity for oxygen reduction reaction, J. Power Sources 314 (2016) 39-48.

[28] L. Guo, J. Deng, G. Wang, Y. Hao, K. Bi, X. Wang, Y. Yang, N, P-doped CoS_2 embedded in TiO_2 nanoporous films for Zn–air batteries, Adv. Funct. Mater. (2018) 1804540 (1 of 8).

[29] T. Wu, M.L. Stone, M.J. Shearer, M.J. Stolt, I.A. Guzei, R.J. Hamers, R. Lu, K. Deng, S. Jin, J.R. Schmidt, Crystallographic facet dependence of the hydrogen evolution reaction on CoPS: theory and experiments, ACS Catal. 8 (2018) 1143-1152.

[30] J. Zhang, Y. Liu, B. Xia, C. Sun, L. Liu, P. Liu, P. Gao, Facile one-step synthesis of phosphorus-doped CoS_2 as efficient electrocatalyst for hydrogen evolution reaction, Electrochim. Acta 259 (2018) 955-961.

[31] C. Ridruejo, F. Alcaide, G. Álvarez, E. Brillas, I. Sirés, On-site H_2O_2 electrogeneration at a CoS_2-based air-diffusion cathode for the electrochemical degradation of organic pollutants, J. Electroanal. Chem. 808 (2018) 364-371.

[32] M. Köck-Schulmeyer, A. Ginebreda, C. Postigo, T. Garrido, J. Fraile, M.L. de Alda, D. Barceló, Four-year advanced monitoring program of polar pesticides in groundwater of Catalonia (NE-Spain), Sci. Total Environ. 470-471 (2014) 1087-1098.

[33] E.T. Rodrigues, M.F. Alpendurada, F. Ramos, M.A. Pardal, Environmental and human health risk indicators for agricultural pesticides in estuaries, Ecotoxicol. Environ. Saf. 150 (2018) 224-231.

[34] J. Dong, D. Li, Z. Peng, Y. Zhou, Synthesis and electrochemical performance of cobalt disulfide, J. Solid State Electrochem. 12 (2008) 171-174.

[35] G. Álvarez, F. Alcaide, P.L. Cabot, M.J. Lázaro, E. Pastor, J. Solla-Gullón, Electrochemical performance of low temperature PEMFC with surface tailored carbon nanofibers as catalyst support, Int. J. Hydrog. Energy 37 (2012) 393-404.

[36] A. Thiam, R. Salazar, E. Brillas, I. Sirés, Electrochemical advanced oxidation of carbofuran in aqueous sulfate and/or chloride media using a flow cell with a RuO_2-based anode and an air-diffusion cathode at pre-pilot scale, Chem. Eng. J. 335 (2018) 133-144.

[37] J.C. Murillo-Sierra, I. Sirés, E. Brillas, E.J. Ruiz-Ruiz, A. Hernández-Ramírez, Advanced oxidation of real sulfamethoxazole + trimethoprim formulations using different anodes and electrolytes, Chemosphere 192 (2018) 225-233.

[38] R.F. Pupo Nogueira, M.C. Oliveira, W.C. Paterlini, Simple and fast spectrophotometric determination of H_2O_2 in photo-Fenton reactions using metavanadate, Talanta 66 (2005) 86-91.

[39] A. Thiam, E. Brillas, F. Centellas, P.L. Cabot, I. Sirés, Electrochemical reactivity of Ponceau 4R (food additive E124) in different electrolytes and batch cells, Electrochim. Acta 173 (2015) 523-533.

[40] W. Xing, G. Yin, G.J. Zhang, (Eds), Rotating Electrode Methods and Oxygen Reduction Electrocatalysts, Elsevier, Amsterdam, NL, 2014.

[41] H. Wang, Y. Liang, Y. Li, H. Dai, $Co_{1-x}S$-graphene hybrid: A high-performance metal chalcogenide electrocatalyst for oxygen reduction, Angew. Chem. Int. Ed. 50 (2011) 10969-10972.

Figure captions

Fig. 1. X-ray diffraction (XRD) patterns of fresh (a) CoS_2/MWCNTs and (b) CoSP/MWCNTs catalysts. These are compared with resulting patterns upon contact with the atmosphere for given periods of time. For comparison, the main signals related to the pyrite-phase of CoS_2 (JCPDS Card No. 41-1471) are presented for each catalyst.

Fig. 2. Changes in the XRD pattern of CoS_2/MWCNTs catalyst at different periods of time when it was preserved under nitrogen atmosphere.

Fig. 3. Selected FE-SEM images of (a) CoS_2/MWCNTs and (b) CoSP/MWCNTs catalysts.

Fig. 4. EDX spectra recorded for fresh (a) CoS_2/MWCNTs and (b) CoSP/MWCNTs catalysts.

Fig. 5. SEM-EDX analysis of CoSP/MWCNTs catalyst, showing the (a) selected scanning area, along with the mapping results for (b) Co, (c) S, and (d) P.

Fig. 6. Cyclic voltammograms recorded using CoSP/MWCNTs in N_2-saturated 0.050 M Na_2SO_4 solution at pH 3.0 and 25 °C: (a) 5^{th} cycle and (b) 10^{th} cycle. (c) Analogous analysis for 10 cycles in O_2-saturated solution. The cell contained a Pt auxiliary electrode and a reversible hydrogen electrode (RHE) as reference electrode. Initial and final potential: -0.170 V; reversal potential: 1.425 V. Scan rate: 20 mV s^{-1}.

Fig. 7. (a) Linear sweep voltammograms obtained with a modified glassy carbon disk as rotating disk electrode (RDE) at rotation rate (rpm) for the reduction of an O_2-saturated 0.050 M Na_2SO_4 solution at pH 3.0 and 25 °C. The cell contained a Pt counter anode, a CoSP/MWCNT-modified working RDE, and a reversible hydrogen electrode (RHE) as reference electrode. Initial potential: 0.840 V; final potential: 0.200 V. Scan rate: 5 mV

s^{-1}. *IR*-drop corrected. (b) Comparative linear sweep voltammograms using a CoS_2/MWCNTs-modified RDE.

Fig. 8. Koutecky-Levich plots obtained from the data of Fig. 7 at 0.250 V vs. RHE for: (a) CoSP/MWCNTs and (b) CoS_2/MWCNTs catalysts. Theoretical linear plots for *n*: (·····) 2 and (– – –) 4 are included for comparison.

Fig. 9. Change of (a) accumulated H_2O_2 concentration and (b) current efficiency with time for the electrolysis of 2.5 L of a 0.050 M Na_2SO_4 solution at pH 3.0 and 35 ºC. A pre-pilot plant containing a filter-press cell with a BDD anode and a (■) CoS_2/MWCNTs, (●) CoSP/MWCNTs or (◆) uncatalyzed MWCNTs air-diffusion cathode, all of 20 cm^2 area, was used, at current density of 25 mA cm^{-2} and liquid flow rate of 180 L h^{-1}. (▲) Results obtained during the photoelectro-Fenton (PEF) treatment of 20 mg L^{-1} bentazon with 0.50 mM Fe^{2+} under the same conditions, using an annular photoreactor with a 160-W UVA lamp.

Fig. 10. Change of (a) bentazon concentration, with the corresponding pseudo-first-order kinetic analysis, and (b) TOC, with the corresponding mineralization current efficiency, with electrolysis time for the treatment of 2.5 L of 20 mg L^{-1} bentazon solutions in 0.050 M Na_2SO_4 at pH 3.0 and 35 ºC. A pre-pilot plant with a CoSP/MWCNTs air-diffusion cathode was used, under the same conditions of Fig. 9. Method: (◆) Electrochemical oxidation with electrogenerated H_2O_2 (EO-H_2O_2) and (▲) PEF with 0.50 mM Fe^{2+} and 160-W UVA radiation.

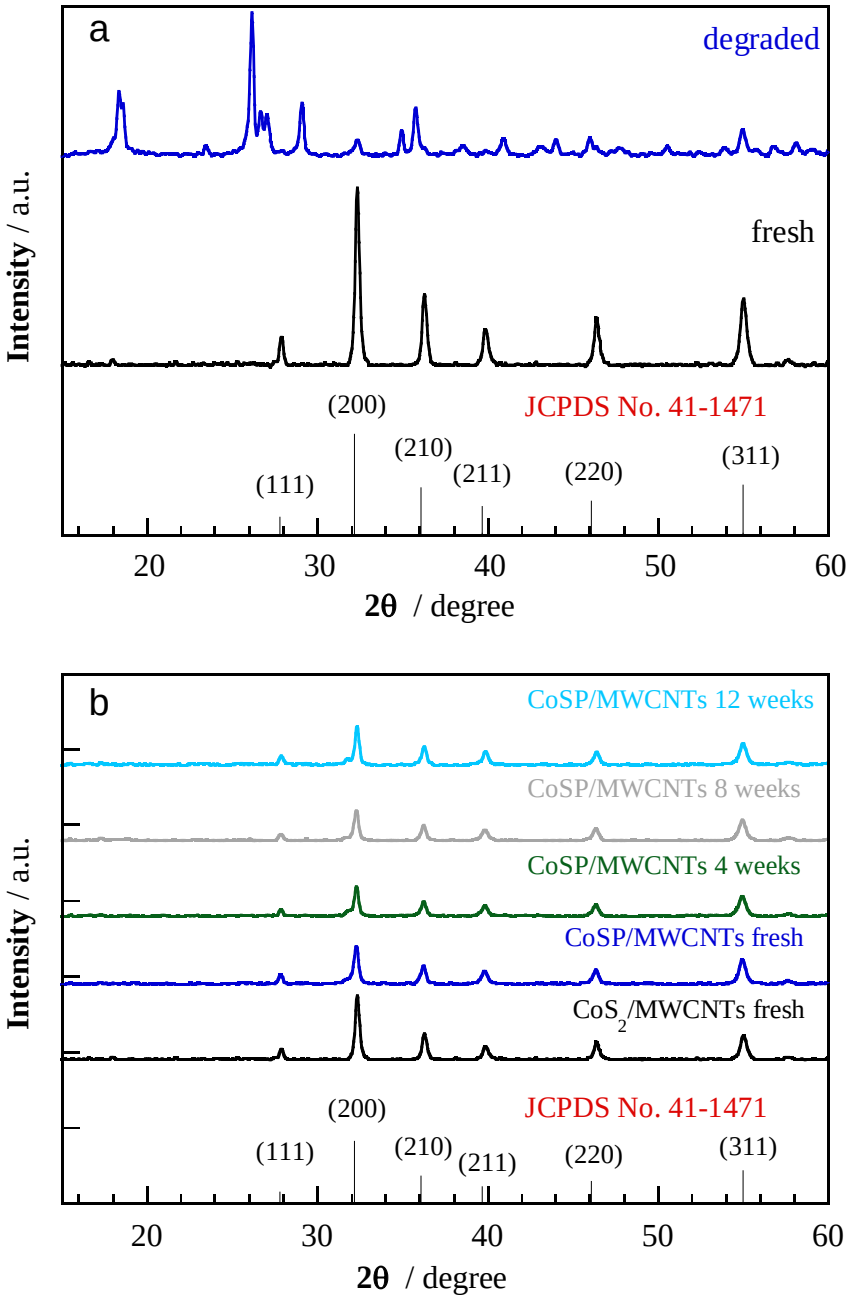
a
degraded
fresh
Intensity / a.u.
(200)
JCPDS No. 41-1471
(210)
(211)
(220)
(311)
(111)
20
30
40
50
60
2θ / degree
b
CoSP/MWCNTs 12 weeks
CoSP/MWCNTs 8 weeks
CoSP/MWCNTs 4 weeks
CoSP/MWCNTs fresh
CoS2/MWCNTs fresh
Intensity / a.u.
(200)
JCPDS No. 41-1471
(111)
(210)
(211)
(220)
(311)
20
30
40
50
60
2θ / degree

Fig. 1

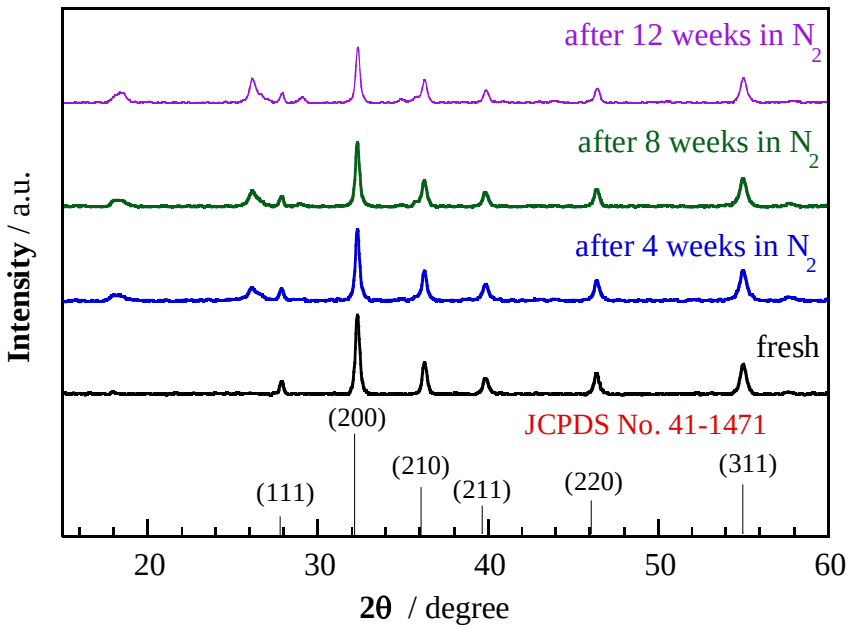
after 12 weeks in N2
after 8 weeks in N2
after 4 weeks in N2
fresh
JCPDS No. 41-1471
(111)
(200)
(210)
(211)
(220)
(311)
Intensity / a.u.
20
30
40
50
60
2θ / degree

Fig. 2

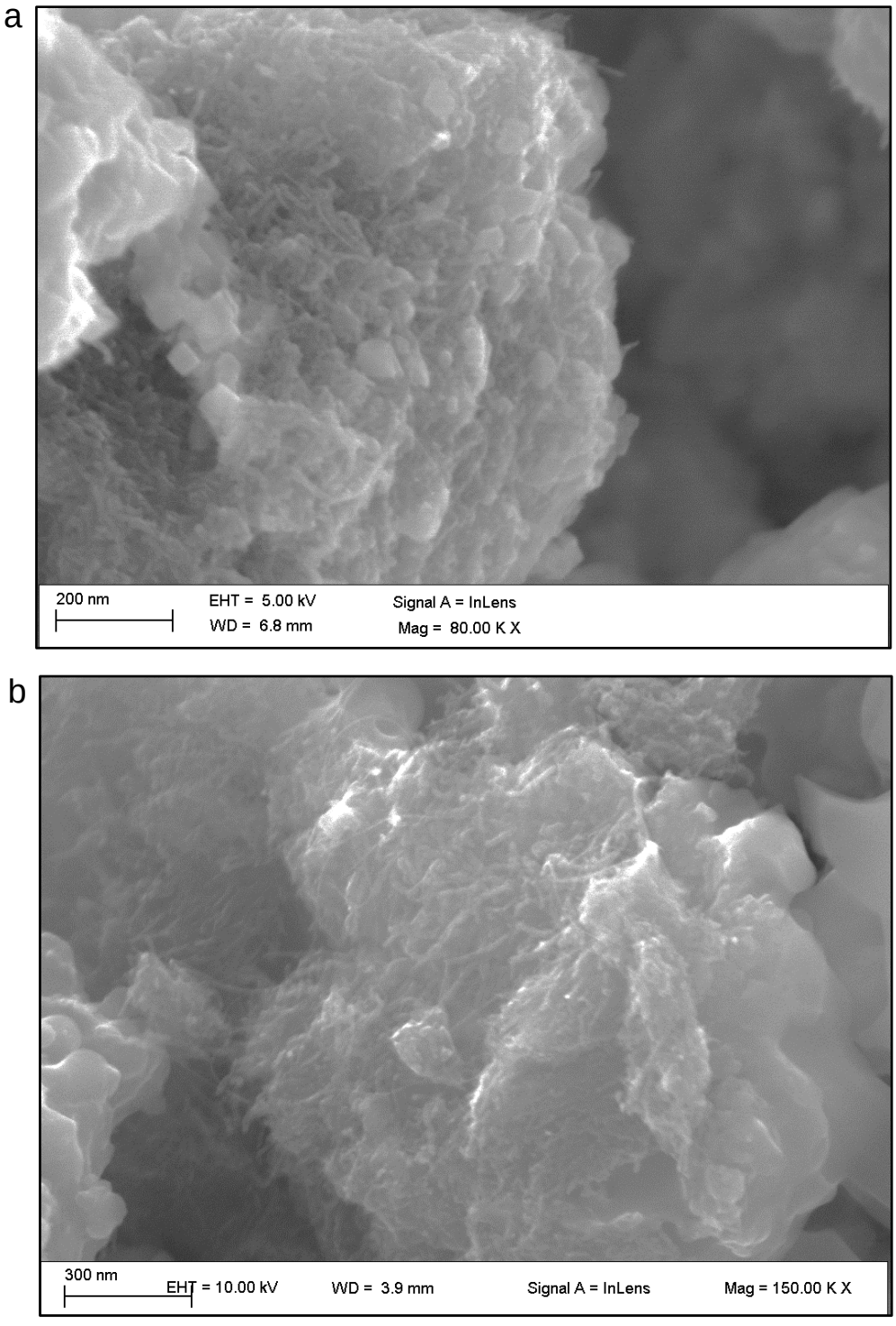
a
200 nm
EHT = 5.00 kV
WD = 6.8 mm
Signal A = InLens
Mag = 80.00 K X
b
300 nm
EHT = 10.00 kV
WD = 3.9 mm
Signal A = InLens
Mag = 150.00 K X

Fig. 3

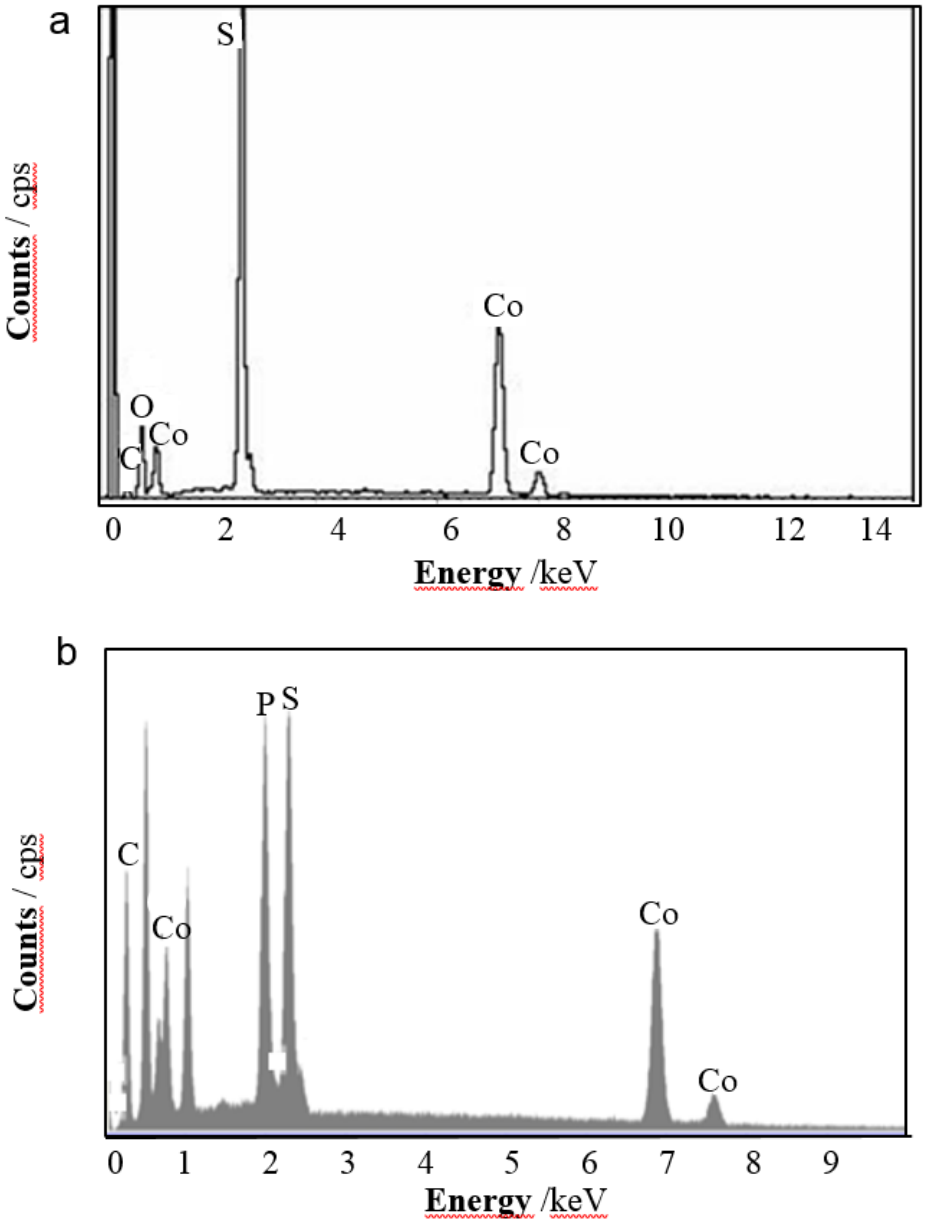
a
S
Co
O
Co
C
Co
Counts / cps
0
2
4
6
8
10
12
14
Energy /keV
b
P S
C
Co
Co
Co
Counts / cps
0
1
2
3
4
5
6
7
8
9
Energy /keV

Fig. 4

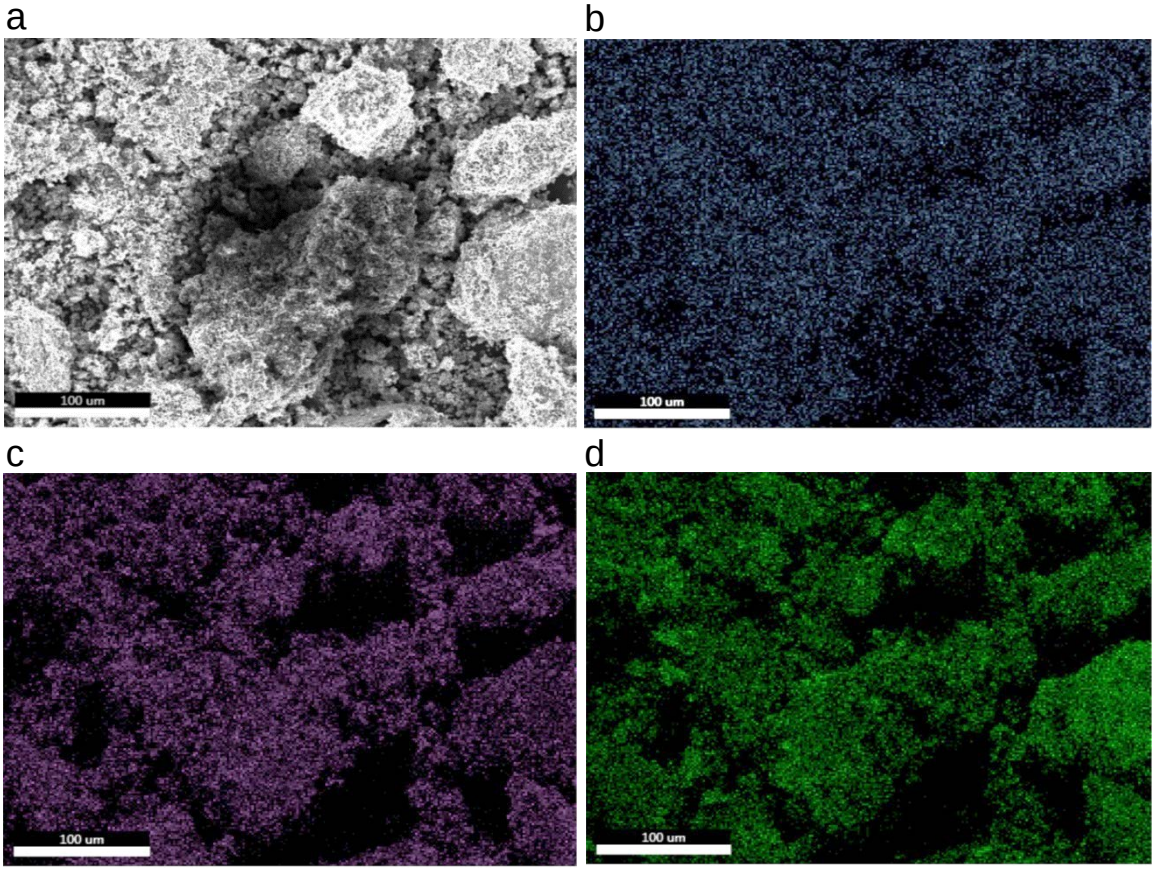

Fig. 5

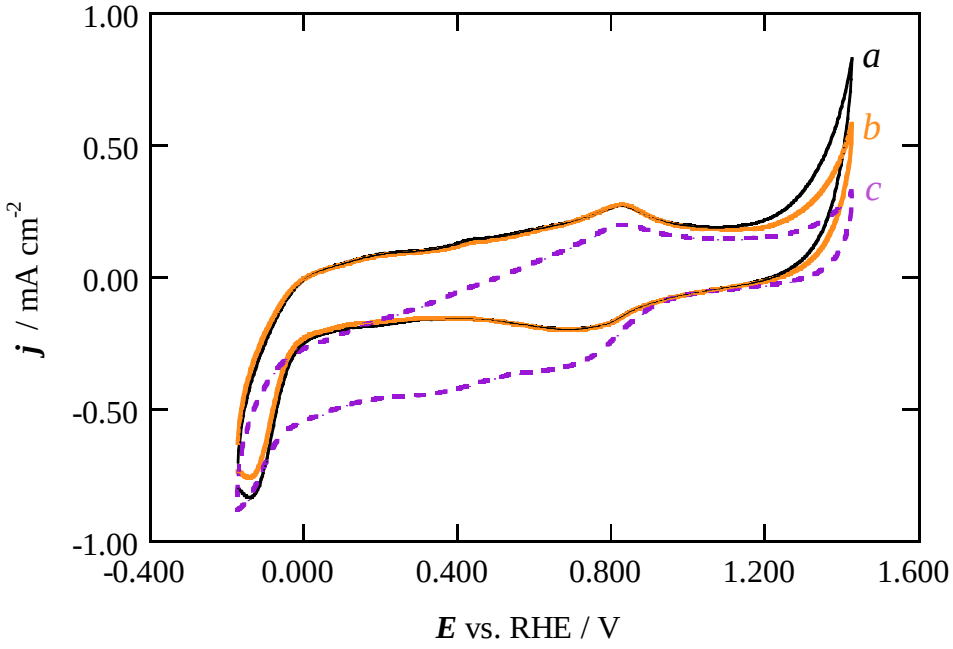
1.00
0.50
0.00
-0.50
-1.00
-0.400
0.000
0.400
0.800
1.200
1.600
j / mA cm-2
E vs. RHE / V
a
b
c

Fig. 6

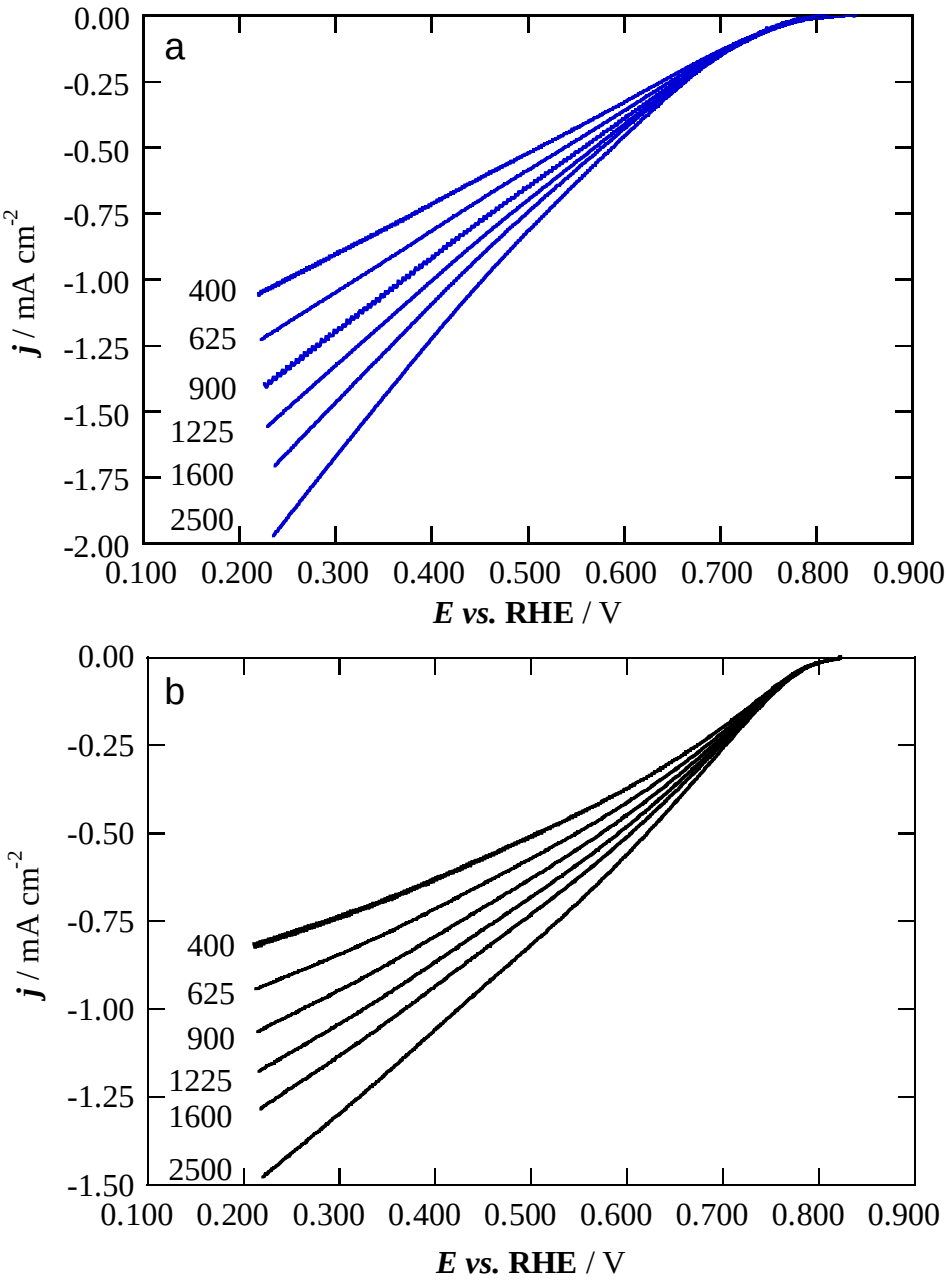
a
0.00
-0.25
-0.50
-0.75
-1.00
-1.25
-1.50
-1.75
-2.00
j / mA cm-2
400
625
900
1225
1600
2500
0.100 0.200 0.300 0.400 0.500 0.600 0.700 0.800 0.900
E vs. RHE / V
b
0.00
-0.25
-0.50
-0.75
-1.00
-1.25
-1.50
j / mA cm-2
400
625
900
1225
1600
2500
0.100 0.200 0.300 0.400 0.500 0.600 0.700 0.800 0.900
E vs. RHE / V

Fig. 7

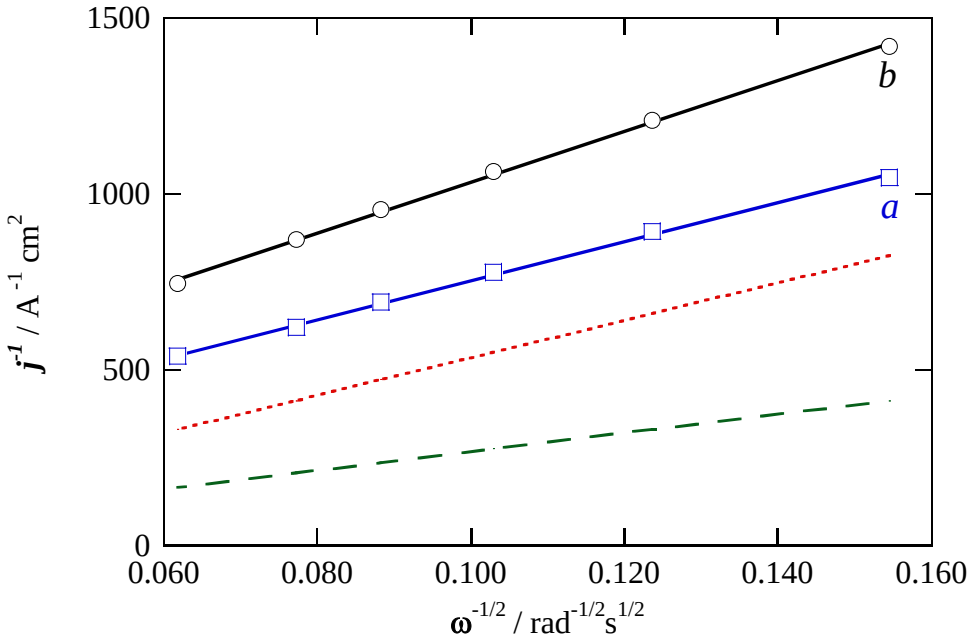
1500
1000
500
0
0.060
0.080
0.100
0.120
0.140
0.160
b
a
j-1 / A-1 cm2
ω-1/2 / rad-1/2s1/2

Fig. 8

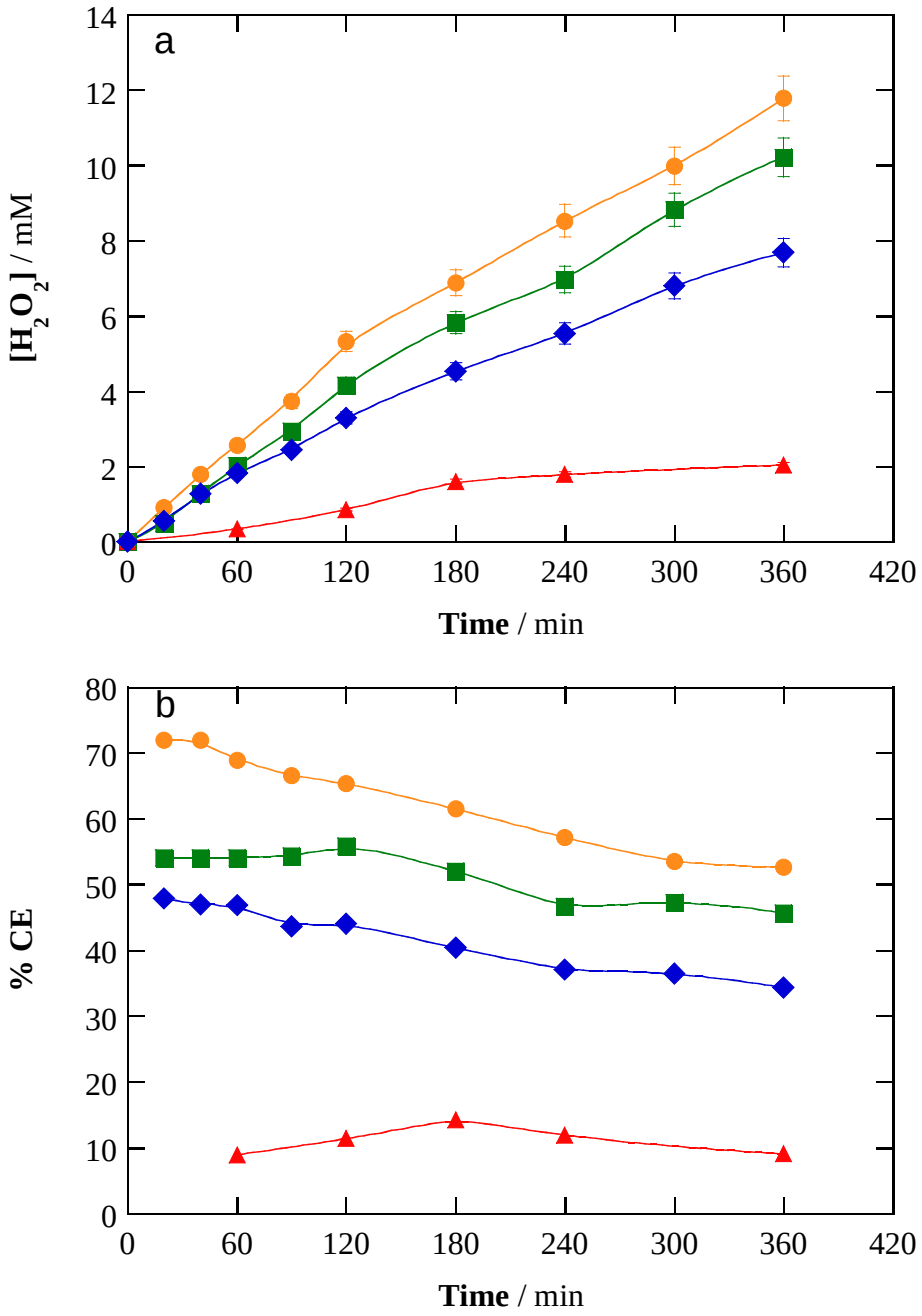

Fig. 9

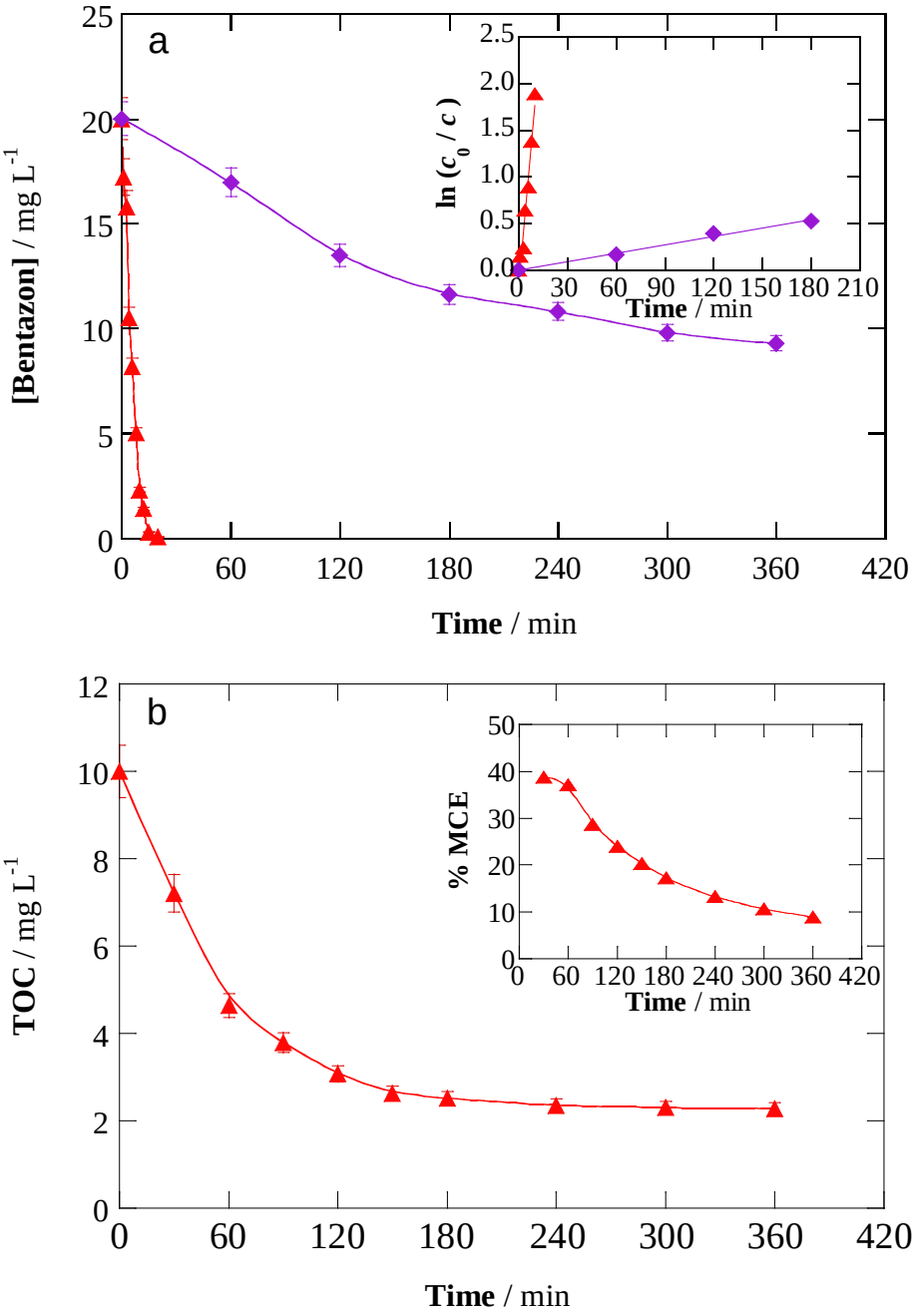
a
[Bentazon] / mg L-1
Time / min
ln (c0 / c)
Time / min
b
TOC / mg L-1
Time / min
% MCE
Time / min

Fig. 10